Macromolecules
ARTICLE

Macromolecules **2010**, *43*, 6127–6134 **6127**
DOI: 10.1021/ma100559u

Characterizing Free Volumes and Layer Structures in Asymmetric Thin-Film Polymeric Membranes in the Wet Condition Using the Variable Monoenergy Slow Positron Beam

Wei-Song Hung,[†] Manuel De Guzman,[†] Shu-Hsien Huang,[§] Kueir-Rarn Lee,*[,†] Y. C. Jean,*[,†,‡] and Juin-Yih Lai[†]

[†]*R&D Center for Membrane Technology, Department of Chemical Engineering, Chung Yuan University, Chung-Li 32023, Taiwan,* [‡]*Department of Chemistry, University of Missouri—Kansas City, Kansas City, Missouri 64110, and* [§]*Department of Chemical and Materials Engineering, National Ilan University, I-Lan 26047, Taiwan*

Received March 12, 2010; Revised Manuscript Received May 14, 2010

ABSTRACT: The free volume sizes and distributions and multilayer structures in asymmetric thin layer polyamide membranes in the wet state have been first time measured using the variable monoenergy slow positron beam (VMSPB). This paper presents a newly developed method which combines the technique of plasma-enhanced chemical vapor deposition to form a barrier layer for high-vacuum condition to seal the composite polyamide and of interfacial polymerization between 2-aminoethanethiol (AETH) and trimesoyl chloride (TMC) on the surface of modified asymmetric polyacrylonitrile (mPAN) membrane (AETH-TMC/mPAN), under the wet condition encountered during the pervaporation process in which they are in direct contact with the liquid environment provided by the feed solution. During the VMSPB experiments under a high vacuum, our new method maintained the thin-film composite (TFC) membrane in the wet conditions typically experienced in VMSPB experiments wherein it directly contacts the liquid feed environment, which is essential in the course of real measurements as there is a high interaction between the feed solution and the membrane. The results of free volumes and layer structures in the wet state are compared with the dry sate and are supported by the results using SEM and FTIT-ATR measurements.

Introduction

A great deal of research in the field of pervaporation has to deal with its application in dehydrating aqueous alcohol solutions.[1−5] To widen this area of application, membranologists have been tailoring different new types of membranes[5,6] with improved characteristics. High-performance pervaporation membranes are specifically based on two criteria: the increase of permeation flux and the enhancement of selectivity. In this respect, asymmetric TFC membranes are a feasible alternative. TFC membranes consist of a thin dense top layer and a porous supporting layer. The permeation flux could be enhanced during the pervaporation measurement, resulting from a thin selective skin layer with a lower mass transfer resistance. Nevertheless, the swelling problem inherently persists regardless of the considerable research efforts and significant advances made or no matter which method is applied to modify membrane materials. Since pervaporation membranes are always in direct contact with the feed solution whose components are to be separated, the membrane inevitably experiences a certain degree of swelling. There is a strong interaction between the feed solution components and the pervaporation membrane. To understand such interaction, it is essential to characterize the membranes' swelling behavior.

Membrane materials used in the pervaporation process are either water or organic solvent permselective. In either case, membranes experience a high swelling at a high concentration of the permeating species. Because of the swelling effect, the membrane selectivity normally suffers:[5,7,8] a reduction of the permselectivity and subsequently leading to a serious problem as far as the selectivity criterion of a suitable pervaporation membrane is concerned. To inhibit the problem on the membranes' high swelling, researchers[7,9] have exhausted in the effort toward producing numerous types of membranes: cross-linked, blended, and organic−inorganic hybrid membranes, etc.

The measurement of the extent of the swelling behavior in TFC membranes encounters technical problems because most conventional instruments available are basically designed for application to free-standing membranes. The methods employed by some studies[1,2] involved peeling off the active layer of the membrane, which is not only invasive but also cumbersome. Furthermore, the conventional instruments are capable of characterizing the composite membrane active layer in its dry state only. The measurements made are, therefore, not representative of the swollen membrane characteristics. With the advent of positron annihilation spectroscopy (PAS),[10] the method with which to determine the swelling behavior of TFC membranes has to be dramatically improved. However, characterizations of composite membranes were still done in their dry state,[10] using the nondestructive PAS and the VMSPB technique.[11] Here, we have developed a new method that enables measurements of the properties of TFC membranes in their wet condition. Then we have been able to appropriately evaluate the swelling behavior in wet TFC membranes. With a newly developed method using a VMSPB, we can determine the relationship between the membrane's real behavior and obtained free volumes. It is essential to elucidate the interaction between pervaporation membranes and feed solutions containing the components to be separated.

*To whom all correspondences should be addressed: Tel +886-3-2654190, Fax +886-3-2654198, e-mail krlee@cycu.edu.tw (K.-R.L.); Tel +816-235-2295, Fax +816-235-5502, e-mail jeany@umkc.edu (Y.C.J.).

Published on Web 06/28/2010

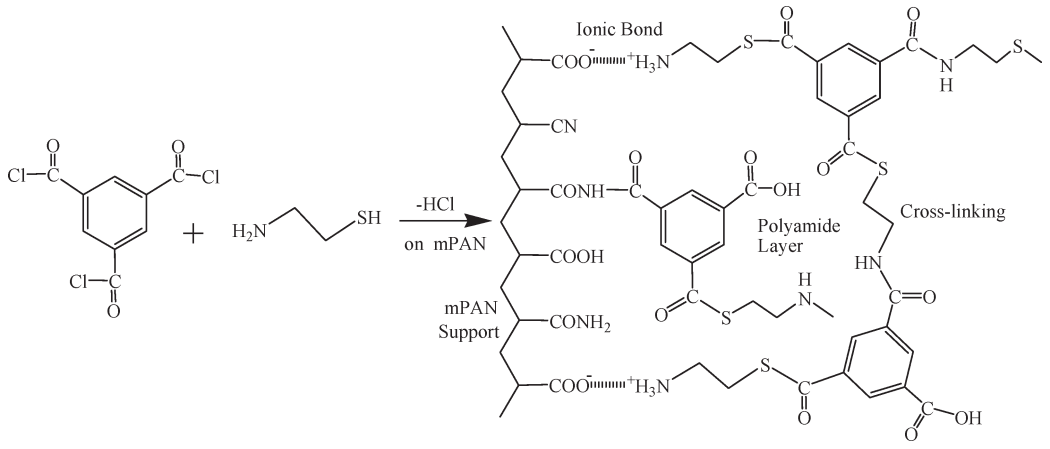

Figure 1. Schematic diagram of chemical reaction and structures for synthesized polyamide from interfacial polymerization between 2-aminoethanethiol (AETH, aqueous phase) reacting with trimesoyl chloride (TMC, oil phase) onto the surface of modified porous polyacrylonitrile (mPAN membrane).

Positron annihilation lifetime spectroscopy (PALS) has been known to be an invaluable tool for investigating local free-volume hole properties in various materials.[10−12] A subnano-order hole radius ranges from around 0.1 to 0.5 nm in radius in the case of polymers and solutions.[10] Orthopositronium (o-Ps, a triplet bound state between a positron and an electron) localized in a free-volume hole can be sensitively detected with PALS measurements. A good correlation between the observed "pick off" o-Ps annihilation lifetime and the cavity size has been rationalized based on a simple quantum mechanical model initially proposed by Tao[13] and later developed by Eldrup et al.[14] and Nakanishi et al.[15] A calibrated semiempirical equation between the observed o-Ps lifetime and the mean free-volume hole size has been established,[13−16] and PALS is the best available technique at present that provides direct information about the size, concentration, and electronic nature of microscopic holes in polymers.[16,17]

To obtain the representative multilayered structure of polyamide composite membranes using VMSPB, it is necessary to keep the membranes in their wet condition. In this study, we present the first successful result to accomplish such requirement by using the method we have developed where we combined the techniques of plasma polymerization and interfacial polymerization to fabricate a plasma-polymerized TFC membrane ($SiO_xC_yH_z$/AETH-TMC/mPAN). The function of the resulting glass-like[18,19] $SiO_xC_yH_z$ layer serves as a protective layer under the high-vacuum condition for the polyamide interfacially polymerized membrane in the wet state. This result demonstrates that PAS, VMSPB, and the developed plasma polymerized methods are applicable to asymmetric membrane systems in the wet state.

Experimental Section

Materials. Polyacrylonitrile (PAN) polymer was supplied by Tong-Hua Synthesis Fiber Co. Ltd. in Taiwan. *N*-Methyl-2-pyrrolidone (NMP) of reagent grade was used as solvent. Trimesoyl chloride (TMC) and 2-aminoethanethiol (AETH) were purchased from TCI Co. Tetraethoxysilane (TEOS) was obtained from ACROS Co. AETH was used as aqueous phase monomer and TMC as organic phase monomer. These two monomers were reacted to carry out the interfacial polymerization process to form an active layer of poly(thiol ester amide). Distilled water was used in preparing aqueous aminothiol solution, and reagent-grade toluene was used as acyl chloride solvent.

Preparation of Modified PAN (mPAN) Porous Support Membrane. Flat porous support membrane was prepared by casting 15 wt % PAN−NMP solutions onto nonwoven polyester fabrics with the use of a 200 μm casting knife. The cast membrane was precipitated by immersion in a bath of water. The resulting PAN porous membrane was washed in water overnight and was then dried at atmospheric conditions. To improve the hydrophilicity of the PAN membrane surface and to facilitate the spread of the aqueous amine solution over it, the PAN membrane was hydrolyzed in a 2 M $NaOH_{(aq)}$ solution at 50 °C. The −CN groups of PAN on the surface of the support membrane can be converted into −COOH groups after the hydrolysis with $NaOH_{(aq)}$ solution. Besides −COOH groups as a product of the hydrolysis, $-CONH_2$ or −CONH groups as byproducts may also form.[20] The resulting modified PAN (mPAN) porous membrane support was washed in a water bath for several hours and was then dried at atmospheric conditions.

Preparation of Polyamide AETH-TMC/mPAN Composite Membrane. The AETH-TMC/mPAN composite membrane was prepared using the technique of the interfacial polymerization between AETH and TMC. The mPAN membrane was first immersed in a 0.01 wt % aqueous aminothiol solution for 10 s. Then, the excess amount of the solution on the membrane surface was removed. This wet membrane with the aminothiol solution was contacted with a 0.05 wt % organic acyl chloride solution for 10 s to carry out the process of interfacial polymerization. The schematic diagram of chemical reaction and structures for synthesized polyamide from interfacial polymerization between 2-aminoethanethiol (AETH, aqueous phase) reacting with trimesoyl chloride (TMC, oil phase) onto the surface of modified porous polyacrylonitrile (m-PAN membrane) is shown in Figure 1.

Preparation of Plasma-Polymerized $SiO_xC_yH_z$/AETH-TMC/mPAN Composite Membrane. The polyamide TFC membrane was fixed on a sample holder for the plasma polymerization process. The sample holder was then placed in a bell-jar-type reactor (Pyrex glass) with external ring electrodes. Prior to plasma deposition, the reactor was evacuated with the use of a rotary and a diffusion pump down to a pressure of 10^{-2} Torr. Then, the process pressure was adjusted to about 0.2 Torr, and the temperature was set at 25 °C. The TEOS monomer flow rate was controlled with electronic mass flow meter at 12.4 mg/min, and the plasma power applied at 150 W. The glass-like plasma polymer thin film of several hundred nanometers was deposited on the polyamide TFC membrane, which served as mechanical support. The prepared $SiO_xC_yH_z$/AETH-TMC/mPAN membrane was assembled together with a front frame and back plate and vacuum-sealed by using epoxy glue. A solvent was injected into the assembled sample holder, directly contacting the membrane so as to maintain it in the wet condition. Details of schematic diagram of sample holder are shown in Figure 2. The assembled $SiO_xC_yH_z$/AETH-TMC/mPAN composite membranes were tested to be vacuum-sealed under the direct

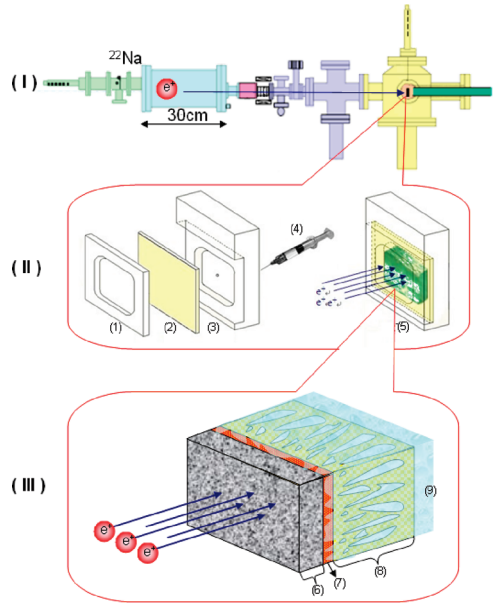

Figure 2. (I) Schematic diagram of variable monoenergy slow positron beam. (II) Detailed schematic diagram of sample holder components: (1) front cover frame, (2) composite membrane, (3) back plate, (4) syringe with solution, and (5) assembled sample holder (components 1−3 glued and together by epoxy). (III) Enlarged diagram of composite membrane: (6) $SiO_xC_yH_z$ layer, (7) AETH-TMC layer, (8) mPAN layer, and (9) solution.

pumping for several hours for characterizing the membrane in its wet state; the assembled sample was then installed into a VMSPB that operates at high vacuum.

Positron Annihilation Spectroscopy. The new VMSPB[21] in the R&D Center for Membrane Technology in Chung Yuan University in Taiwan was used for this study to define the mean depth of the membrane between 0 and about 10 μm (the mean depth was determined by converting the positron incident energy from 0 to 30 keV using an established equation[22]). This new radioisotope beam uses 50 mCi of ^{22}Na as the positron source. Two positron annihilation spectrometers were connected to the beam, namely Doppler broadening energy spectroscope (DBES) and positron annihilation lifetime spectroscope (PALS), which use the secondary electrons emitted from the sample surface as starting signal. The DBES spectra were measured using an HP Ge detector at a counting rate of ~2000 cps. The energy resolution of the solid-state detector was 1.5 keV at 0.511 MeV (corresponding to the positron 2γ annihilation peak). The total number of counts for a DBES spectrum was 1.0 million.

When a positron enters the polymeric surface, it loses its energy via inelastic collision processes within the time scale of 10^{-12} s, and its energy distribution could be expressed by a Makhovian implantation profile. The mean depth of the polymeric materials where the positron annihilation occurs could be calculated from positron incident energy using an established equation[10,12,22] which also depends on the density of materials. It is worthwhile to note that since the positron energy spreads as soon as the positron enters the sample, and the data obtained is a superposition of distribution possibly into multilayers. The current PAS technique has not achieved to the stage of complete deconvolution of all positron data as a function of depth except in the multilayer (up to 5 layers) analysis of *S* parameter where we used the available VEPFIT program, which deconvolutes the data correctly by using the Makhovian implantation profile (see Results and Discussion section).

The PALS data were obtained by taking the coincident events between the start signal detected by a multichannel plate (MCP) from the secondary electrons and the stop signal by a BaF_2 detector form the annihilation photons at a counting rate of approximately 200−300 cps. A PALS spectrum contains 2.0 million counts.

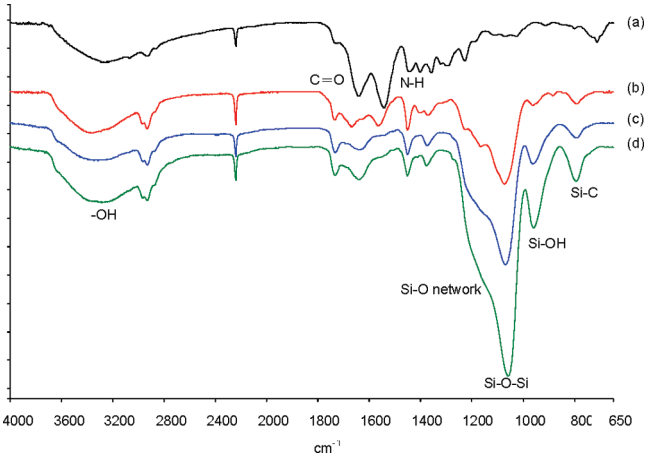

Figure 3. ATR-FTIR spectra for TFC membrane (a) and plasma-polymerized $SiO_xC_yH_z$/AETH-TMC/mPAN composite membranes at different deposition times of 0.5 (b), 1 (c), and 2 h (d) (system pressure: 0.2 Torr; TEOS flow rate: 12.4 mg/min; RF power: 150 W).

Surface and Morphological Characterization. Various analytical methods were used to characterize the chemical and physical properties of the plasma-polymerized $SiO_xC_yH_z$ layers. The morphologies of the $SiO_xC_yH_z$ /AETH-TMC/mPAN membranes were analyzed with scanning electron microscopy (SEM, Hitachi model S4700). FTIR-ATR (Perkin-Elmer, model SPECTRUM ONE) was used to investigate the change in the chemical components of the $SiO_xC_yH_z$ layers.

Results and Discussion

Characterization of the $SiO_xC_yH_z$/AETH-TMC/mPAN Composite Membrane. Figure 3 shows the ATR-FTIR spectrum for the AETH-TMC/mPAN membrane and the spectra for the plasma-polymerized $SiO_xC_yH_z$ layers produced at different deposition times.

The AETH-TMC/mPAN membrane spectrum was taken to confirm whether the active layer of the membrane was composed of polyamide. We can see in Figure 3a two peaks corresponding to C=O (amide I) and N−H (amide II) at wavenumbers of 1653 and 1569 cm^{-1}, respectively. The presence of these peaks validates that the AETH-TMC/mPAN composite membrane consists of the polyamide layer.[23]

The spectra for $SiO_xC_yH_z$ layers (Figure 3b−d) were obtained to provide evidence as to the deposition of plasma-polymerized films on top of the polyamide active layer of the AETH-TMC/mPAN composite membrane. These spectra indicate a strong absorption peak due to Si−O−Si stretching vibration at 1059 cm^{-1}, weak absorption peaks due to Si−OH and Si−C groups at 932 and 819 cm^{-1}, respectively, and a shoulder at 1160 cm^{-1}. This shoulder can be explained to be due to extrinsic distortions of Si−O networks by impurities such as carbon and silanol groups.[23,24] We have demonstrated that the film formed as a result of the plasma-induced deposition of the TEOS monomer consists mainly of Si−O networks with a small amount of Si−OH and Si−C groups.

A comparison of the spectrum for the AETH-TMC/mPAN membrane and the spectra for the plasma-polymerized $SiO_xC_yH_z$ layers reveals the following. (1) The polyamide C=O and N−H peaks are not observed in the spectra for the plasma-polymerized layers, suggesting that the polyamide surface was covered with $SiO_xC_yH_z$ layers completely. (2) The amount of $SiO_xC_yH_z$ layers seems to be increasing with deposition times proceeding from 0.5 to 2 h. This

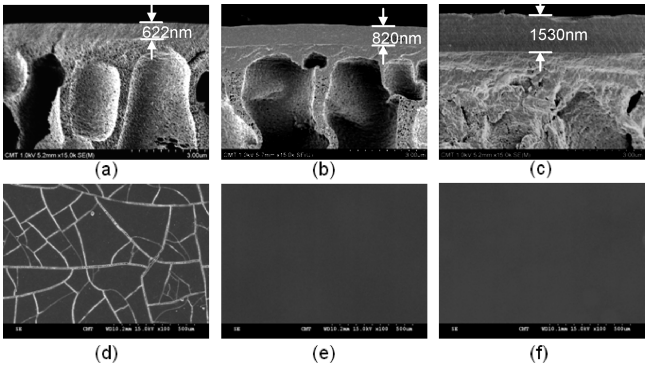

Figure 4. SEM pictures of plasma-polymerized $SiO_xC_yH_z$/AETH-TMC/mPAN composite membranes. Cross-sectional images in the first row and surface images in the second row. Deposition times: (a, d) 0.5 h; (b, e) 1 h; (c, f) 2 h.

observation was based on the increasing intensity of the Si−O−Si peak at 1059 cm^{-1}; the polyamide layer seems to be gradually covered with increasing amount of the deposited $SiO_xC_yH_z$ layer, resulting in a protective layer form on the AETH-TMC/mPAN membrane surface. Figure 4a−c clearly illustrates that the plasma layer thickness increased with the deposition time. These data provide evidence for the increasing amount of the deposited film on the polyamide TFC membrane. In addition, from Figure 4a, we obtained the layer thickness as a result of plasma polymerization for 0.5 h to be 622 nm. This thickness is not sufficient or strong to prevent the solvent from evaporating (the solvent was contained in the sample holder installed in the VMSPB that operates at high vacuum), resulting from the presence of surface cracks on the deposited $SiO_xC_yH_z$ layer (Figure 4d). From Figure 4e,f, the layer thicknesses after 1 and 2 h of plasma deposition are determined to be 820 and 1530 nm, respectively. Both of these layers have the mechanical strength and sufficient thickness to protect the active layer of the composite membrane and to seal the high vacuum well, as evident by the unaffected dense film surface (no cracks). The solvent in the mPAN side of assemble did not evaporate at high-vacuum conditions of the VMSPB because the protective thick $SiO_xC_yH_z$ layer held sufficient strength.

From the above discussion, we conclude that the plasma-deposited film on the TFC membrane is capable of maintaining the membrane in the wet state under a high-vacuum system of VMSPB when the layer thickness is 820 nm or thicker. The following results of positron experiments were obtained from the plasma-polymerized AETH-TMC/mPAN wet composite membrane assemble with $SiO_xC_yH_z$ layer thickness of 820 nm (corresponding to a deposition time of 1 h).

Swelling Behavior Influence on the Free Volume of $SiO_xC_yH_z$/AETH-TMC/mPAN Composite Membrane. Experiments on positron annihilation spectroscopy (PAS) coupled with a VMSPB were performed as a function of positron energy form 100 eV to 30 keV in both dry and the wet $SiO_xC_yH_z$/AETH-TMC/mPAN composite membrane. Both Doppler broadening energy spectra (DBES) and positron annihilation lifetime spectra (PALS) were measured to obtain the depth profiles and the free volume information.

DBES is a powerful technique for observing the physical microstructural change of materials based on measuring the relative width of the annihilation photons with energy near 511 keV. A parameter given by DBES is called the *S* parameter, which is defined as the ratio of the central part of the annihilation spectrum to the total spectrum. The *S* parameter represents positron annihilation with low momentum

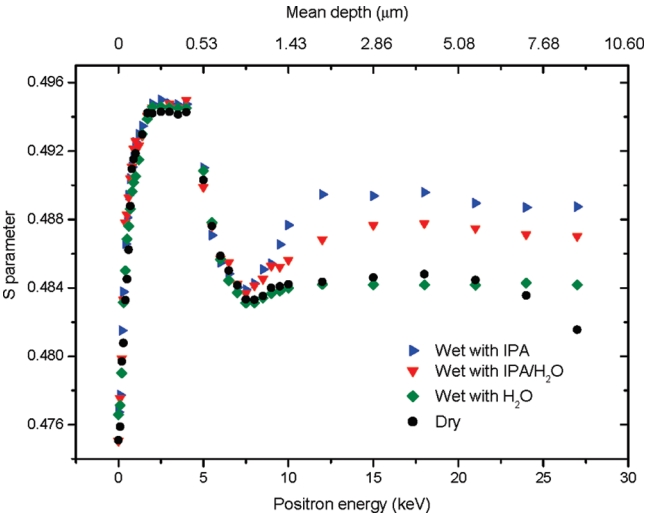

Figure 5. *S* parameter as a function of positron incident energy or mean depth in dry and wet states of plasma-polymerized $SiO_xC_yH_z$/AETH-TMC/mPAN composite membranes. Solvents used to keep membranes wet: IPA, 70 wt % IPA/H_2O, and H_2O.

valence electrons.[25−27] The variation in the *S* parameter reveal the variation in the free volumes and the multilayer structures in asymmetric polymeric materials and membranes.[11,22,23]

Figure 5 shows the *S* parameter as a function of the positron energy (or the mean depth) for $SiO_xC_yH_z$/AETH-TMC/mPAN composite membrane both in the dry and wet states.

From this plot, we observe the changes in the *S* value as a function of the increasing positron incident energy as follows: (1) From nearly zero positron energy or a point near the plasma-polymerized layer surface, the *S* value increases steeply at the surface (from the vacuum). (2) Then, the *S* value exhibits a plateau at some distance from the layer surface toward the interface between the inorganic ($SiO_xC_yH_z$) layer and the organic (AETH-TMC polyamide layer) composite membrane. (3) Next, the *S* value decreases steeply across the interface until a valley is reached. (4) Further, the *S* value increases and exhibits another plateau. (5) The last trend of the change in the *S* value applies for all the TFC membranes soaked with different types of solvent. The maximum *S* values that reach the plateaus attained for each composite membrane are different. However, for the dry composite membrane, the *S* value eventually decreases slightly after a plateau.

The above observations in Figure 5 could be interpreted as follows. First, the initial increase in the *S* parameter very near the inorganic $SiO_xC_yH_z$ layer surface is due to back diffusion and scattering of positronium (Ps) and positrons back to vacuum from a point of very small implantation depth measured from the layer surface. The sharp increase of *S* is due to the short diffusion length of the Ps (∼nm) and the positrons (∼10−100 nm) in the highly defected the inorganic ($SiO_xC_yH_z$) coated layer.[11,28] Second, when the positron penetrates into the bulk of the plasma-polymerized $SiO_xC_yH_z$ layer, the *S* parameter displays an approximately constant value of 0.492 ± 0.001 for both the dry and wet composite membranes probed by the VMSPB. The large *S* value in this region is consistent with that published in the literature.[28] A nearly constant *S* value indicates that the major part of this layer is with a structure of the inorganic $SiO_xC_yH_z$ layer, which would not be easily swollen by the solvent in direct contact with the composite membrane. Third, the transition

layer, as demarcated in Figure 5, from 4.5 to 6.8 keV is from the coated oxide layer to the polyamide and mPAN membrane. The decrease of S is due to the smaller free volumes in polyamide[11] than coated oxides or mPAN base in the interfacial regions. This transition layer then reaches the AETH-TMC polyamide layer of the TFC membrane, which is estimated to be at 7.5 keV. It is known that S values for organic TFC membranes are lower than the S value for the $SiO_xC_yH_z$ layer.[10,29] And this is the case for the S values shown in Figure 5 for all TFC membranes. Fourth, the next to the polyamide layer is the mPAN skin layer and then porous mPAN. The significant variation of S starts to occur at the positron energy greater than 7.5 keV. This variation could be interpreted due to the strong interaction between the solvent and the polyamide/mPAN membranes. S values for the wet composite membrane samples differ from those for the dry one. In the case of the wet TFC membrane samples, the S values increased in the following order of the solvent that kept the membrane wet: isopropanol > 70 wt % IPA/H_2O > water. It could be interpreted in the following possibility: the isopropanol has a larger τ_3 (3.6 ns; with intensity 20%) than water τ_3 (1.8 ns; with intensity 20%). A larger swelling leads to a larger S value. The swelling effect caused by isopropanol is greater than water. The polymer chains in the swollen region are more flexible, and the energy required for the solvent diffusive transport is less. In addition, the extent of swelling caused by water is much less than isopropanol, as the S values for the TFC membrane wet with water are approximately the same as those for the dry membrane (see Figure 5). A slight decrease of the S values for the dry TFC membrane decreased after attaining a plateau at about 18 keV is probably due to the inhomogeneous pore distribution of mPAN (pore size several micrometers) as seen in the SEM cross section.

It is interesting that the absorption of solvent is clearly identified from another R parameter in DBES spectra. The R parameter is taken as a ratio between the total count in the γ-ray energy between 364.2 and 496.2 keV (3γ annihilation) and that near the 511 keV (504.3−517.6 keV for 2γ annihilation) region. The R parameter provides information about the existence of large pores (nm to μm), where o-Ps undergoes 3γ annihilation. In general, the S parameter obtained by means of analyzing 2γ annihilation is a relative value that represents a composite measure primarily from free volume quantity (based on p-Ps annihilation) and secondarily from size (based on the uncertainty principle)[11,22,26] for free volumes and defects ranging from an Å to 1 nm. From the section mapping by means of SEM observation, the mPAN substrate contains a big portion of macrovoid (pore) structure pore sizes in the micrometer range, which reduces the relative quantity of free volumes and nanoscale defects, and thus has a smaller S value in Figure 5. However, data on mPAN large pores can be mirrored from Figure 6 based on the R values (3γ annihilation in nm to μm range of pores). A detailed description of the R parameter measurement can be found elsewhere.[11,22]

We can observe from the R plot high values of R near the $SiO_xC_yH_z$ layer surface due to 3γ annihilation in the beam and in the region pertaining to the dry membrane (7−27 keV). These R values for the dry membrane are due to the contribution of o-Ps from the pore in the membrane starting from 7 keV, which is a point in the positron energy outside the region of the $SiO_xC_yH_z$ layer network. The increasing R parameter between 7 and 13 keV is identified as the transition layer between the AETH-TMC polyamide and dense skin layer of mPAN membrane support. The R plateau from a layer depth greater than 15 keV corresponds

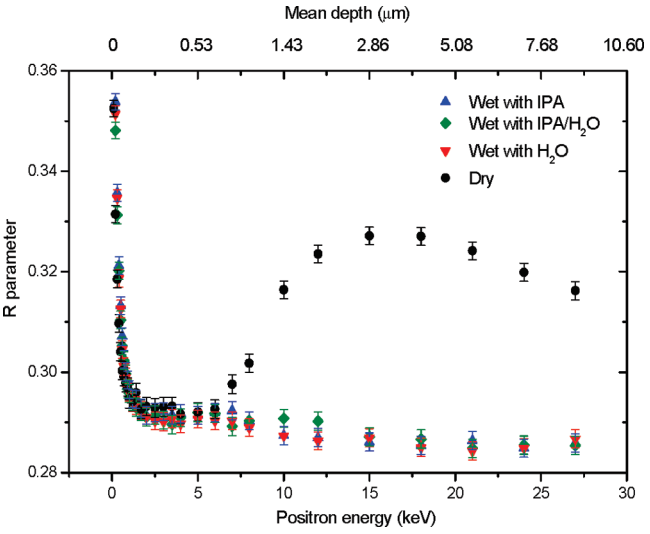

Figure 6. R parameter as a function of positron incident energy or mean depth at dry and wet states of plasma-polymerized $SiO_xC_yH_z$/AETH-TMC/mPAN composite membranes. Solvents used to keep membranes wet: IPA, 70 wt % IPA/H_2O, and H_2O.

to the contribution from large pores (μm) due to 3γ annihilation of o-Ps.

For the wet membranes, high R values are only seen in the region near the $SiO_xC_yH_z$ surface (which is due to back scattering and diffusion of Ps and positrons[12,22]), and the R values in the transition and mPAN layers region slightly decrease. There are no high R values in the S in the wet membranes, as indicated by a small R value for the $SiO_xC_yH_z$ layer and in the wet TFC membranes. The interesting phenomenon of low and nearly constant R values for the wet membranes may be ascribed to the solvent-filled membranes, and this condition inhibits 3γ annihilation.

Analysis of Free Volumes in Plasma-Polymerized $SiO_xC_yH_z$/AETH-TMC/mPAN Composite Membrane. We have performed the positron PALS for the $SiO_xC_yH_z$/AETH-TMC/mPAN composite membrane at selected positron energies of 2−15 keV. The obtained raw PALS spectra are shown in Figure 7. In the PALS data obtained using a slow positron beam like us, we have analyzed data in both three- and four-lifetime components using the PATFIT program.[30] This is because there exists a long o-Ps component contributed from the Ps and positron back-diffused and scattered from the surface of the samples and also in large pores in the membranes.[10,11] Therefore, in slow beam PALS data analysis using PATFIT, we consistently found that the four-lifetime analysis gives better χ^2 values and stable with reasonable errors than three-lifetime analysis. The lifetime and intensity results are summarized in Table 1. The longest lifetimes ($\tau_4 \sim 30-100$ ns) are attributed to the o-Ps lifetimes in the pores (> nm) and in the beam chamber, and they are not sensitive for pore analysis at μm region. The τ_3 and its intensity are useful information for the free volume information in membranes. The lifetime τ_3 and intensity I_3 vary significantly as a function of the incident positron energy because of different layer structures, chemical compositions, and material properties at various depths from the $SiO_xC_yH_z$ layer surface. Each PAL spectrum gives two short positron lifetime components ($\tau_1 \sim 0.2$ ns and $\tau_2 \sim 0.5$ ns) are due to p-Ps (singlet Ps state) annihilation and positron (unbounded) annihilations which are not sensitive enough for free volume determination. At a given positron energy, a PALS spectrum, τ_3 and intensity I_3 are used to determine free volumes and layer structures in the plasma-polymerized

$SiO_xC_yH_z$/AETH-TMC/mPAN composite membrane. For example, the spectra between 2 and 6 keV of positron implantation energies correspond to the $SiO_xC_yH_z$ layer. For these spectra (plotted with square and round symbols in Figure 7), the slopes of the long-live component (τ_3) are nearly similar because the plasma-polymerized $SiO_xC_yH_z$ layer has similar physical and chemical structures. The PALS spectrum at 7.5 keV implantation energy (plotted with upright triangle symbol in Figure 7) corresponds to the polyamide layer (AETH-TMC). Compared with the PAL spectrum at 2 and 6 keV implantation energies, the long-lived component of the PAL spectrum at 7.5 keV implantation energy has a sharp slope, a reasonable indicator that the layer structure transfer from inorganic region ($SiO_xC_yH_z$) to organic region (AETH-TMC). The spectra at 9 and 15 keV implantation energies (plotted with inverted triangle and diamond symbols in Figure 7) represent the AETH-TMC + mPAN skin layer and the porous layer in the mPAN support, respectively.

The observed slope of the long-lived component for the former spectrum (9 keV) is higher than the latter (15 keV). These phenomena could be attributed to the microstructural relaxation property of the porous mPAN compared to the AETH-TMC + mPAN skin layer part of the TFC membrane.

The analyzed results of τ_3 and intensity I_3 as a function of the positron energy for $SiO_xC_yH_z$/AETH-TMC/mPAN composite membrane in the dry state and the wet condition (using 70 wt % aqueous isopropanol solution as solvent) are shown in Figure 8.

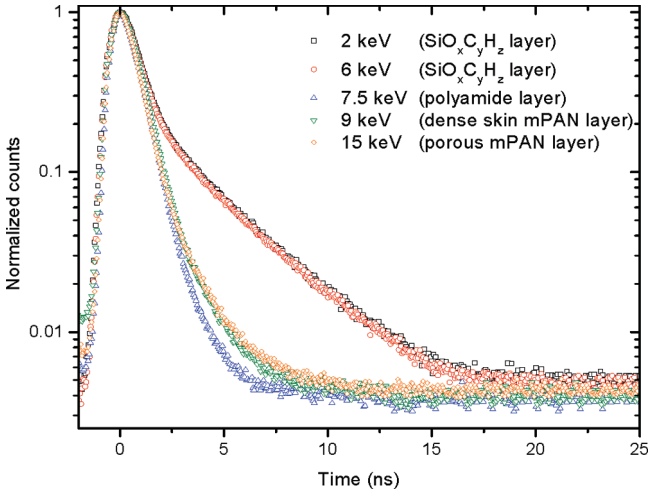

Figure 7. Normalized positron annihilation lifetime (PAL) spectra at different positron incident energies for plasma-polymerized $SiO_xC_yH_z$/AETH-TMC/mPAN composite membranes maintained in the wet state with 70 wt % IPA/H_2O solvent.

The variations in τ_3 and I_3 in Figure 8 are described as follows. (1) A sharp increase in I_3 near the $SiO_xC_yH_z$ layer surface is observed. This is a general phenomenon for short diffusion lengths of Ps in highly defected materials. This trend of sharp increase near the layer surface was also observed in the S variation shown in Figure 5 because S reflects the p-Ps. (2) τ_3 values and variation as a function of layer depth can be used to interpret the material types, since inorganic and organic materials have different o-Ps pick-off annihilation lifetimes. For a layer depth corresponding to the 1−6.5 keV range, τ_3 is constant at 2.1 ± 0.1 ns (radius = 2.9 Å). The I_3 curve for this region exhibited a plateau with an intensity of 35%, indicating a homogeneous structure of the $SiO_xC_yH_z$ layer network.[31] (3) The next change in I_3 after reaching plateau is a sharp decrease, crossing a transition from the $SiO_xC_yH_z$ layer (0−6.5 keV) to the AETH-TMC/mPAN composite membrane layer (7−15 keV). For τ_3 in the dry TFC membrane layer, we observed a valley in the τ_3 curve equivalent to 1.83 ± 0.05 ns (radius = 2.69 Å) at 7.5 keV and then an increase in τ_3 to a plateau of 2.2 ns (radius = 3.0 Å). This is the trend that we would expect for a transition from AETH-TMC polyamide to mPAN dense skin layer because the free volume in the former is smaller than that in the latter.[32] (4) The identification of the AETH-TMC polyamide to mPAN dense skin layer in the dry TFC membrane layer is further supported by the observed I_3

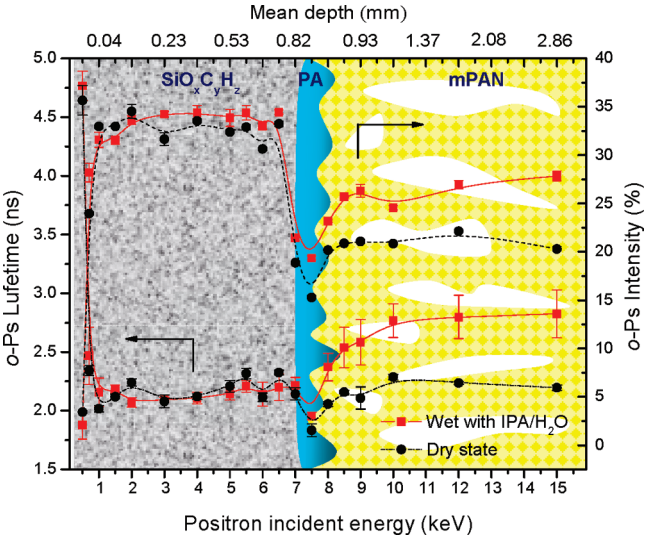

Figure 8. o-Ps annihilation lifetime (τ_3) and intensity (I_3) vs positron incident energy or mean depth for plasma-polymerized $SiO_xC_yH_z$/AETH-TMC/mPAN composite membranes in dry state and wet conditions (using 70 wt % IPA/H_2O as solvent). Lines drawn through data are to guide the eye only.

Table 1. Positron Lifetime Results at Different Positron Incident Energies for $SiO_xC_yH_z$/AETH-TMC/mPAN Membrane Systems in the Wet and Dry States[a]

positron incident energies	τ_2 (ns)	I_2 (%)	τ_3 (ns)	I_3 (%)	τ_4 (ns)	I_4 (%)	R_f (Å)[b]	FFV (%)[b]
2 keV ($SiO_xC_yH_z$ layer) dry	0.457 ± 0.013	52.34 ± 0.88	2.241 ± 0.030	34.53 ± 0.73	61.5 ± 4.1	1.247 ± 0.347	3.07 ± 0.02	7.51 ± 0.31
2 keV ($SiO_xC_yH_z$ layer) wet	0.428 ± 0.008	55.50 ± 0.47	2.069 ± 0.038	33.62 ± 0.45	57.9 ± 2.4	1.646 ± 0.522	2.92 ± 0.03	6.29 ± 0.26
6 keV ($SiO_xC_yH_z$ layer) dry	0.408 ± 0.057	57.31 ± 0.21	2.114 ± 0.036	30.65 ± 0.18	60.8 ± 3.7	1.835 ± 0.270	2.96 ± 0.03	5.98 ± 0.19
6 keV ($SiO_xC_yH_z$ layer) wet	0.471 ± 0.011	53.97 ± 0.53	2.139 ± 0.101	33.02 ± 0.36	64.2 ± 4.4	1.425 ± 0.767	2.98 ± 0.07	6.58 ± 0.54
7.5 keV (polyamide layer) dry	0.409 ± 0.022	54.38 ± 0.73	1.833 ± 0.054	15.23 ± 0.18	39.5 ± 5.2	0.314 ± 0.334	2.69 ± 0.05	2.25 ± 0.14
7.5 keV (polyamide layer) wet	0.422 ± 0.014	52.82 ± 0.58	1.954 ± 0.034	19.35 ± 0.19	54.6 ± 3.8	0.129 ± 0.218	2.81 ± 0.03	3.25 ± 0.12
9 keV (skin mPAN layer) dry	0.447 ± 0.013	56.67 ± 0.31	2.108 ± 0.094	21.07 ± 0.17	67.7 ± 2.3	0.595 ± 0.483	2.95 ± 0.07	4.09 ± 0.31
9 keV (skin mPAN layer) wet	0.486 ± 0.008	53.36 ± 0.74	2.583 ± 0.194	26.30 ± 0.66	76.5 ± 5.8	0.705 ± 0.094	3.34 ± 0.11	7.38 ± 0.91
15 keV (porous mPAN layer) dry	0.477 ± 0.013	50.34 ± 0.13	2.195 ± 0.023	20.31 ± 0.23	74.9 ± 7.2	0.829 ± 0.547	3.03 ± 0.02	4.25 ± 0.11
15 keV (porous mPAN layer) wet	0.445 ± 0.007	51.64 ± 0.81	2.825 ± 0.205	27.84 ± 0.52	87.7 ± 6.1	0.705 ± 0.094	3.52 ± 0.10	9.13 ± 0.97

[a] The shortest lifetime time τ_1 was fixed to 0.125 ns in PATFIT analysis. [b] R_f and FFV are the mean free-volume radius and the relative free-volume fractions, respectively, estimated from o-Ps data according to semiempirical equations.[13−16]

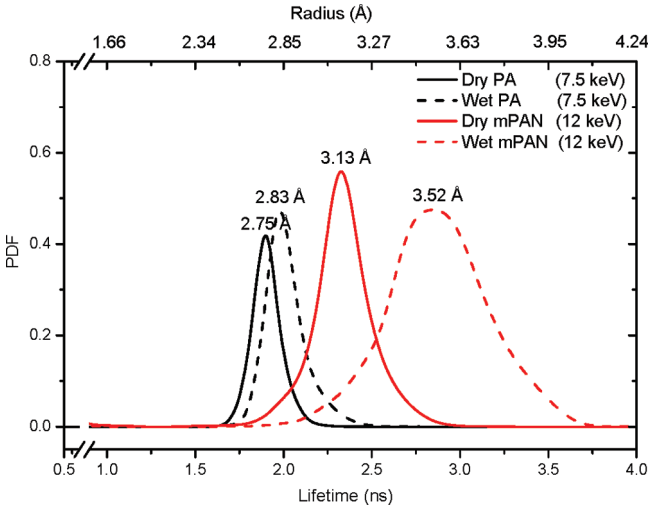

Figure 9. Mean free-volume radius and o-Ps lifetime distributions for plasma-polymerized $SiO_xC_yH_z$/AETH-TMC/mPAN composite membranes in the dry and wet states. Values indicated at peaks in each distribution curve are mean radii obtained from MELT[33] analysis of mean lifetimes.

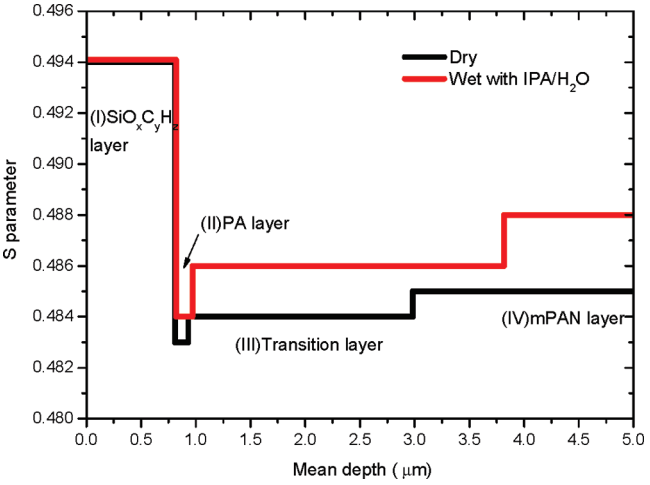

Figure 10. Schematic diagram of four-layer depth structure obtained by using VEPFIT program analysis of *S* parameter data from DBES in $SiO_xC_yH_z$/AETH-TMC/mPAN composite membranes. Description of four layers: (I) plasma-polymerized $SiO_xC_yH_z$ layer, (II) interfacially polymerized polyamide (PA) layer, (III) transition layer from dense skin to porous support layer of mPAN, and (IV) porous support layer of mPAN.

increase from 15.3 to 20.2%, which is a similar trend observed in the *S* value vs depth plot in Figure 5. In addition, the results for the TFC membrane in the wet state have the same trend as the dry membrane. The important information we observed is that the τ_3 and I_3 for the membrane in the wet state are higher than those for the membrane in the dry state. For example, in the AETH-TMC polyamide layer, the o-Ps lifetime for the dry and wet state membranes at 7.5 keV implantation energy are 1.83 ns (radius = 2.69 Å) and 1.95 ns (radius = 2.80 Å), respectively. The o-Ps intensity for the dry and wet state membranes at the same implantation energy is 15.3% and 19.3%, respectively. These differences between the dry and wet membranes can be attributed to the greater swelling in the wet membranes, leading to the expansion of the existing free volumes and the creation of more free volumes, such as plastizing effect. The welling effect has increased the observed lifetime as well as the intensity. The swelling effect in the dense AETH-TMC polyamide layer (7−7.5 keV) being less than in the mPAN support layer (higher than 7.5 keV), which is more hydrophobic. This may be interpreted due to the aromatic TMC having a rigid phenyl ring and three acyl chloride groups. Cross-linking network structure could be established in the AETH-TMC active layer formed from reacting AETH with TMC, resulting in a more stable polyamide layer on the TFC membrane and in a weak swelling effect from its contact with 70 wt % isopropanol/water solutions. Furthermore, the hydrophilicity of the mPAN membrane is much high than that of the AETH-TMC active layer, resulting from the PAN membrane was hydrolyzed in a 2 M $NaOH_{(aq)}$ solution. The −CN groups of PAN on the surface of the support membrane can be converted into −COOH, $-CONH_2$, or −CONH groups after the hydrolysis with $NaOH_{(aq)}$ solution, leading to increased hydrophilicity, and thus the mPAN layer relative to the PA layer is more likely to undergo swelling.

We further analyzed the obtained PALS spectra into continuous lifetimes for the free-volume distribution information using the MELT program.[33] The results of free-volume radius and its distribution for both dry and wet plasma-polymerized $SiO_xC_yH_z$/AETH-TMC/mPAN composite membranes (70 wt % IPA/H_2O was used as solvent for the wet state membrane) at positron energies of 7.5 and 12 keV are shown in Figure 9 as probability distribution function (PDF) vs lifetime data.

The shapes of the resulting o-Ps lifetime distribution curves are similar. A comparison of both lifetime values and distribution widths for porous mPAN layer (12 keV) and AETH-TMC polyamide layers (7.5 keV) reveals that the distributions in the wet state membranes are broader than the dry state membranes. From the currently reported PAS experiments, we demonstrated a newly developed nondestructive approach for characterizing wet composite membranes.

From the results of the PALS analysis, *S* parameter, and *R* parameter vs depth and with the aid of SEM images, we identified the multilayered structure of the plasma-polymerized $SiO_xC_yH_z$/AETH-TMC/mPAN composite membrane. It is worthwhile to affirm that the skin layer thickness from PAS data and SEM images showed a consistent result. Additional information from the *S*/*R* parameters and PALS data analysis includes the layer thickness of inorganic and organic materials, the porosity or density as a function of layer depth, and the identification of the transition layer between the skin and porous layers. PALS data could provide a quantitative analysis of free-volume size and intensity as a function of layer depth after analyzing the results using a VEPFIT program[34] to deconvolute the positron energy into an implantation profile. In the process of multilayer analysis, we tried to fit three-, four-, and five-layer models in the VEPFIT program. The three-layer model could not give reasonably good χ^2 values (>4), whereas the five-layer model gave slightly better χ^2 values than the four-layer model, but the fitted results were unstable and the resultant errors were larger than the fitted layer thicknesses and diffusion lengths. During the VEPFIT fitting process, we found appropriate fitting results descriptive of a four-layer model (Figure 10): based on consistent good χ^2 values (<1.9) and reasonable errors. We therefore reported the results of four-layer analysis in this paper. The four layers indicated are as follows: (I) plasma-polymerized $SiO_xC_yH_z$ layer, (II) interfacially polymerized polyamide layer, (III) transition layer from dense skin to porous support layer of mPAN, and (IV) porous support layer of mPAN. The fitting results data for each layer are tabulated in Table 2.

Table 2. Data Obtained from Analysis of Multilayered Structure of $SiO_xC_yH_z$/AETH-TMC/mPAN Composite Membrane[a]

								density (g/cm^3)			
sample	S_1	S_2	S_3	S_4	L_1 (nm)	L_2 (nm)	L_3 (nm)	ρ_1	ρ_2	ρ_3	ρ_4
dry	0.494 ± 0.001	0.483 ± 0.001	0.484 ± 0.001	0.485 ± 0.001	815 ± 153	116 ± 37	2051 ± 973	1.1 ± 0.1	1.2 ± 0.1	1.0 ± 0.1	0.8 ± 0.1
wet with IPA/H_2O	0.494 ± 0.001	0.484 ± 0.001	0.486 ± 0.001	0.488 ± 0.001	817 ± 217	153 ± 84	2847 ± 2059	1.1 ± 0.1	1.2 ± 0.1	1.0 ± 0.1	0.8 ± 0.1

[a] L_1, L_2, and L_3 are the respective thicknesses of layers I−III deduced from the fitted S data analysis using the VEPFIT program. ρ_1, ρ_2, ρ_3, and ρ_4 are the densities of each layer in the composite membrane.

The data show that for layer I S_1 (~0.494) and L_1 (~816 nm) for the $SiO_xC_yH_z$ layer in the dry and wet states reveal similar results, which can be attributed to the difficulty for the solvent to easily penetrate the dense inorganic $SiO_xC_yH_z$ layer. For layers II and III, the wet membrane S parameter values and layer thicknesses are greater than the dry membrane. This implies that solvent effects induce greater polymer swelling and subsequently chain disentanglement in the wet membrane, thereby increasing the free volume mobility and the layer thickness. The densities in Table 2 were the best fitted (judging χ^2) from the results in the VEPFIT program analysis by varying input density values. The values of ρ_2, ρ_3, and ρ_4 agree with previously reported;[11] however, ρ_1 is smaller than that reported in the literature (1.5−2.2 g/cm^3).[24,35] The lower density in our system indicates that the current coated oxide layer has a highly amount of close pores. The observed transition layer in the wet membrane, which was not been observed previously by other techniques,[36,37] has a thickness on the order of a few micrometers. This measured transition layer thickness will be useful in theoretical developments for mass transport phenomena in asymmetric membrane systems.

Conclusion

We have reported the results of free volume size, distribution, and multilayer structure for a polyamide TPC membrane in the wet state using a VMSPB operating in a high-vacuum condition and by using the plasma polymerization process in depositing a 820 nm coated inorganic $SiO_xC_yH_z$ layer. The free volume results show an expansion of free volumes and a broadening of distributions in the wet state compared with the dry membrane. The resolved multilayer structures indicate that wetted polyamide and transition layers are larger than the dry membrane. These results demonstrate that positron annihilation spectroscopy in using a VMSPB is applicable to asymmetric membrane systems in the wet state.

Acknowledgment. The authors sincerely thank the project Toward Sustainable Green Technology in Chung Yuan University, Taiwan, under Grant CYCU-98-CR-CE, the Ministry of Economic Affairs, the Ministry of Education Affairs, and the National Science Council of Taiwan for financially supporting this work.

References and Notes

(1) Freger, V. *Environ. Sci. Technol.* **2004**, *38*, 3168–3175.
(2) Satyanarayana, S. V.; Subrahmanyam, V. S.; Verma, H. C.; Sharma, A.; Bhattacharya, P. K. *Polymer* **2006**, *47*, 1300–1307.
(3) Lee, K. R.; Teng, M. Y.; Lee, H. H.; Lai, J. Y. *J. Membr. Sci.* **2000**, *164*, 13–23.
(4) Hwang, S. T.; Kammermeyer, K. In *Membrane in Separation*; John Wiley Sons: New York, 1975.
(5) Baker, R. W. In *Membrane Technology and Applications*; McGraw-Hill Companies: New York, 2000.
(6) Smitha, B.; Suhanya, D.; Sridhar, S.; Ramakrishna, M. *J. Membr. Sci.* **2004**, *241*, 1–21.
(7) Uragami, T.; Okazaki, K.; Matsugi, H.; Miyata, T. *Macromolecules* **2002**, *35*, 9156–9163.
(8) Uragami, T.; Matsugi, H.; Miyata, T. *Macromolecules* **2005**, *38*, 8440–8446.
(9) Mulder, M. In *Basic Principles of Membrane Technology*; Kluwer Academic Publisher: Dordrecht, 1996.
(10) Jean, Y. C.; Mallon, P. E.; Schrader, D. M. In *Principles and Applications of Positron and Positronium Chemistry*; World Scientific: Singapore, 2003.
(11) Chen, H. M.; Hung, W. S.; Lo, C. H.; Huang, S. H.; Cheng, M. L.; Liu, G.; Lee, K. R.; Lai, J. Y.; Sun, Y. M.; Hu, C. C.; Suzuki, R.; Ohdaira, T.; Oshima, N.; Jean, Y. C. *Macromolecules* **2007**, *40*, 7542–7557.
(12) Nagel, C.; Gunther-Schade, K.; Fritsch, D.; Strunskus, T.; Faupel, F. *Macromolecules* **2002**, *35*, 2071–2077.
(13) Tao, S. J. *J. Chem. Phys.* **1972**, *56*, 5499–5510.
(14) Eldrup, M.; Lightbody, D.; Sherwood, J. N. *Chem. Phys.* **1981**, *63*, 51–58.
(15) Nakanishi, N.; Wang, S. J.; Jean, Y. C. In *Positron Annihilation Studies of Fluids*; Sharma, S. C., Ed.; World Scientific: Singapore, 1988; p 292.
(16) Jean, Y. C. *Microchem. J.* **1990**, *42*, 72–102.
(17) Jansen, J. C.; Macchione, M.; De Lorenzo, L.; Tocci, E.; Yampolskii, Y. P.; Sanfirova, O.; Shantarovich, V. P.; Heuchel, M.; Hofmann, D.; Drioli, E. *Macromolecules* **2009**, *42*, 7589–7604.
(18) Huang, H. H.; Orler, B.; Wilkes, G. L. *Polym. Bull.* **1985**, *14*, 557–564.
(19) Erlat, A. G.; Spontak, R. J.; Clarke, R. P.; Robinson, T. C.; Haaland, P. D.; Tropsha, Y.; Harvey, N. G.; Vogler, E. A. *J. Phys. Chem. B* **1999**, *103*, 6047–6055.
(20) Oh, N. W.; Jegal, J.; Lee, K. H. *J. Appl. Polym. Sci.* **2001**, *80*, 2729–2736.
(21) Hung, W. S.; Lo, C. H.; Cheng, M. L.; Chen, H. M.; Liu, G.; Chakka, L.; Landa, D.; Tung, K. L.; Huang, S. H.; Lee, K. R.; Sun, Y. M.; Yu, C. C.; Zhang, R.; Jean, Y. C. *Apply. Surf. Sci.* **2008**, *255*, 201–204.
(22) Coleman, P. G. In *Positron Beams and Their Application*; World Scientific: Singapore, 2000.
(23) Huang, S. H.; Lin, W. L.; Liaw, D. J.; Li, C. L.; Kao, S. T.; Wang, D. M.; Lee, K. R.; Lai, J. Y. *J. Membr. Sci.* **2008**, *322*, 139–145.
(24) Inagaki, N.; Tasaka, S.; Makino, M. *J. Appl. Polym. Sci.* **1997**, *64*, 1031–1039.
(25) Kobayashi, Y.; Kojima, I.; Hishita, S.; Suzuki, T.; Asari, E. K., M. *Phys. Rev. B* **1995**, *52*, 823–828.
(26) Jean, Y. C.; Zhang, R.; Cao, H.; Yuan, J.-P.; Huang, C.-M.; Nielsen, B.; P., A.-K. *Phys. Rev. B* **1997**, *56*, 8459–8462.
(27) Li, Y.; Zhang, R.; Chen, H.; Zhang, J.; Suzuki, R.; Ohdaira, T.; Feldstein, M. M.; Jean, Y. C. *Biomacromolecules* **2003**, *4*, 1856–1864.
(28) Yu, R. S.; Ito, K.; Hirata, K.; Sato, K.; Zheng, W.; Kobayashi, Y. *Chem. Phys. Lett.* **2003**, *379*, 359–363.
(29) Suzuki, R.; Ohdaira, T.; Uedono, A.; Kobayashi, Y. *Appl. Surf. Sci.* **2002**, *194*, 89–96.
(30) Kirkegaard, P.; Pederson, N. J.; Eldrup, M. PATFIT package, Riso National Laboratory, Roskilde, 1989.
(31) Ito, K.; Oka, T.; Kobayashi, Y.; Suzuki, R.; Ohdaira, T. *Radiat. Phys. Chem.* **2007**, *76*, 213–216.
(32) Huang, S. H.; Hung, W. S.; Liaw, D. J.; Li, C. L.; Kao, S. T.; Wang, D. M.; De Guzman, M.; Hu, C. C.; Jean, Y. C.; Lee, K. R.; Lai, J. Y. *Macromolecules* **2008**, *41*, 6438–6443.
(33) Shukla, A.; Peter, M.; Hoffman, L. *Nucl. Instrum. Methods Phys. Res., Sect. A* **1993**, *335*, 310–317.
(34) Van Veen, A.; Schut, H. H.; de Vries, J.; Hakvoort, H. A.; IJpma, M. R. *AIP Conf. Proc.* **1990**, *218*, 171–193.
(35) Roualdes, S.; Lee, A. V. d.; Berjoan, R.; Sanchez, J.; Durand, J. *AIChE J.* **1999**, *45*, 1566–1575.
(36) Gudernatsch, W.; Menzel, T.; Strathmann, H. *J. Membr. Sci.* **1991**, *61*, 19–30.
(37) Shi, E.; Huang, W.; Xiao, Z.; Li, D.; Tang, M. *J. Appl. Polym. Sci.* **2007**, *104*, 2468–2477.